

Manual for the Processing of MARSIS Electron Density Profiles

by

D. D. Morgan, E. Nielsen, and O. Witasse

I. Introduction

The recent public availability of MARSIS ionogram data has created an interest, among researchers in the Mars Express community and beyond, in learning the processes used to analyze topside sounder ionograms. This document is intended as a ready reference, a “cookbook,” to enable researchers inexperienced in the theory and practice of ionogram inversion to make use of the mass of data currently becoming available. The authors all have experience in the processes of taking the required data and inverting it to get the density profile.

This document will comprise six sections in addition to this introduction. The second section will briefly discuss the basic structure of the MARSIS ionogram data. Each remaining section will discuss, with a minimum of detail, the procedures for completing the major steps of the inversion process. The sections are

1. General introduction.
2. An introduction to the sounding data.
3. Acquisition of the spacecraft altitude and plasma frequency local to the spacecraft. These data provide an essential “anchor point” on which the remaining steps are based.
4. Acquisition of the ionospheric traces—delay time as a function of sounding frequency.
5. Processing of the trace, for example, smoothing out the “stair step” pattern that is a result of the instrumental resolution and removal of data points corrupted by noise.
6. Inversion of the trace; that is, converting from delay time as a function of frequency to altitude as a function of density.
7. A summary of any caveats or pitfalls that exist in this process.

II. Introduction to MARSIS Topside Ionospheric Sounding Data

The smallest usable unit of data from the MARSIS ionospheric sounder is an ionogram. An ionogram consists of an array of received power color coded and plotted as a function of the sounding frequency and the delay time. An example of an ionogram is shown in Fig. 1.

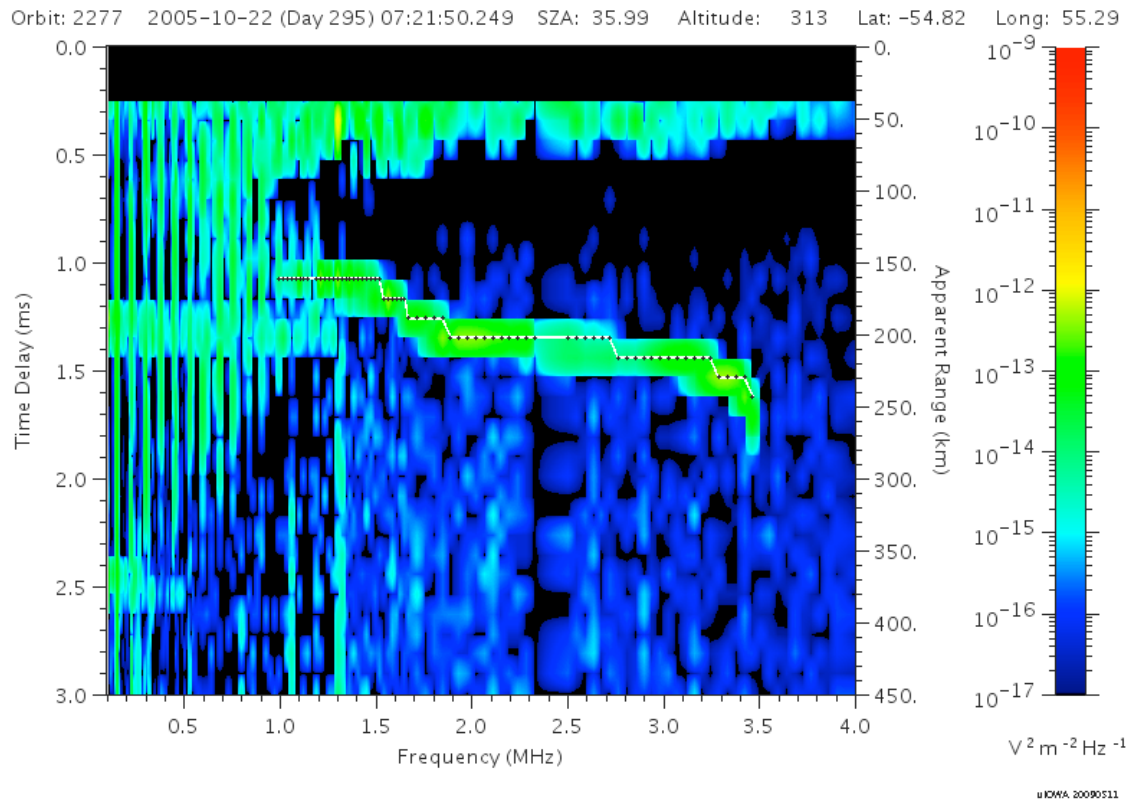


Fig. 1. An ionogram from MARSIS AIS, with received intensity (color code) plotted against sounding frequency (x-axis) and delay time (left-hand y-axis) or apparent range from the spacecraft (right-hand y-axis). Vertical lines in the upper left-hand corner are harmonics of the spacecraft-local plasma frequency due to distortion effects in the receiver. The mostly horizontal structure centered in the figure marked with a dotted line is the ionospheric echo. As discussed in the text, the “stairstep” effect of the ionospheric echo is due to the 91.4- μ s resolution in delay time (13.8 km resolution in apparent range).

In Fig. 1, the x-axis shows values of the sounding frequency. The left-hand y-axis gives delay time, while the right-hand y-axis gives the apparent range, *i. e.*, the calculated range from the spacecraft assuming no dispersion due to plasma. The color coding

indicates the received intensity of the reflected wave. The descending bright line centered in the figure is the sounding echo from the Martian ionosphere. The vertical bright lines at low frequency are an instrumental effect that gives us the plasma frequency local to the Mars Express spacecraft. We shall discuss the use of these signals in subsequent sections.

A complete ionogram is an array of 160 frequencies (ranging from 0.1 to 5.5 MHz) \times 80 delay times (of the form $t_{\text{delay}} = 162.5 + 91.4 + i*91.4 \mu\text{s}$, $0 \leq i \leq 79$, at the i th time point, and ranging from 253.9 to 7565.9 μs) against values of the received intensity, which correspond to the mapped colors. The values of the sampled frequency table underwent revision early in the mission but have remained constant since 14 August 2005. The final and current frequency table is given in Table 1:

Table 1

109.37700	120.48500	131.16700	142.27500
152.95600	175.17400	185.85500	196.96300
207.64500	218.75300	229.86200	240.54300
251.65200	273.44200	284.55000	295.23200
306.34000	317.02100	328.13000	339.23900
349.92000	361.02800	371.71000	382.81800
393.92700	404.60800	415.71700	426.39800
437.50700	448.61500	459.29700	470.40500
481.08600	492.19500	503.30400	513.98500
525.09300	535.77500	546.88300	557.99200
568.67300	579.78200	601.57200	623.36200
645.15100	667.36900	689.15800	710.94800
732.73800	754.52800	776.31800	808.36200
820.32500	842.11500	863.90500	885.69500
907.91200	929.70200	951.49200	973.28100
995.07100	1017.28800	1039.07800	1082.65800
1104.44800	1126.66500	1148.45500	1170.24500
1202.28900	1213.82500	1236.04200	1257.83200

1279.62200	1323.20100	1345.41800	1367.20800
1388.99800	1410.78800	1432.57800	1454.79500
1476.58500	1498.37500	1520.16500	1541.95500
1564.17200	1585.96200	1607.75200	1629.54100
1651.33100	1673.54800	1717.12800	1760.70800
1804.71500	1848.29500	1892.30200	1935.88200
1979.46100	2023.46800	2067.04800	2110.62800
2154.63500	2198.21500	2242.22200	2285.80100
2329.38100	2373.38800	2416.96800	2460.97500
2504.55500	2548.13500	2592.14200	2635.72100
2679.72800	2723.30800	2766.88800	2810.89500
2854.47500	2898.48200	2942.06100	2985.64100
3029.64800	3073.22800	3117.23500	3160.81500
3204.39500	3248.40200	3291.98100	3335.98800
3379.56800	3423.14800	3467.15500	3510.73500
3554.31400	3598.32200	3641.90100	3685.90800
3729.48800	3773.06800	3817.07500	3860.65500
3904.66200	3991.82100	4079.40800	4166.99500
4254.58200	4342.16800	4429.32800	4516.91500
4604.50100	4692.08800	4779.67500	4866.83500
4954.42100	5042.00800	5129.59500	5216.75400
5304.34100	5391.92800	5479.51500	5501.30500

Figure 2 shows the difference between adjacent sounding frequencies as a function of the sounding frequency. The error bars indicate the bandwidth of the frequency sample, which is constant at 10 kHz. Early in the mission, the frequency sampling table was modified to its present quasi-logarithmic because the original sampling frequencies did not provide enough resolution at frequencies below 2 MHz. It is precisely at low frequencies that high resolution is needed, because this is where the density changes rapidly with altitude. Figure 3 shows the spacing of the sounding frequencies normalized by the sounding frequency. This figure shows that, for frequencies greater than about

500 kHz, the frequency spacing is less than 5% of the frequency. In this frequency range, the average fractional spacing is about 2%.

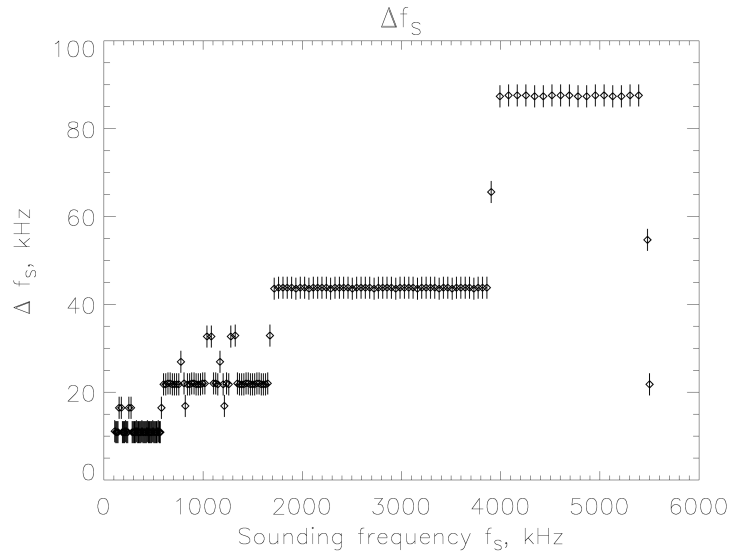


Fig. 2. The MARSIS AIS sounding frequency table (x-axis) and frequency spacing (y-axis). The error bars are ± 5 kHz, the bandwidth of the measurement.

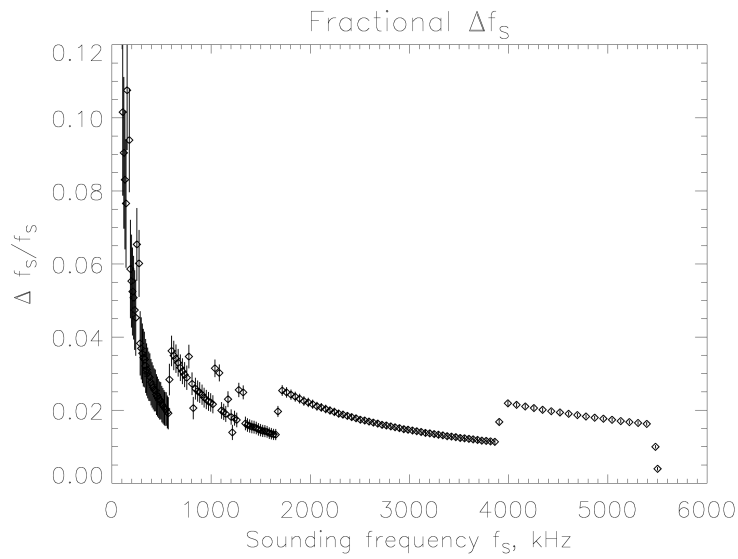


Fig. 3. The MARSIS AIS sounding frequency table (x-axis) and fractional frequency spacing (y-axis). The error bars are $\pm 5 \text{ kHz}/f_s$, the bandwidth of the measurement normalized by the sounding frequency f_s .

III. The Spacecraft Local Plasma Frequency

In the processing of an ionospheric trace, the corrected range for each data point is dependent on the plasma density profile of the ray path previously traversed by the sounding wave. In the case of a topside sounder, this implies the plasma density at the spacecraft is an essential piece of information. In this section, we show the method by which the spacecraft-local electron plasma frequency can in many cases be obtained.

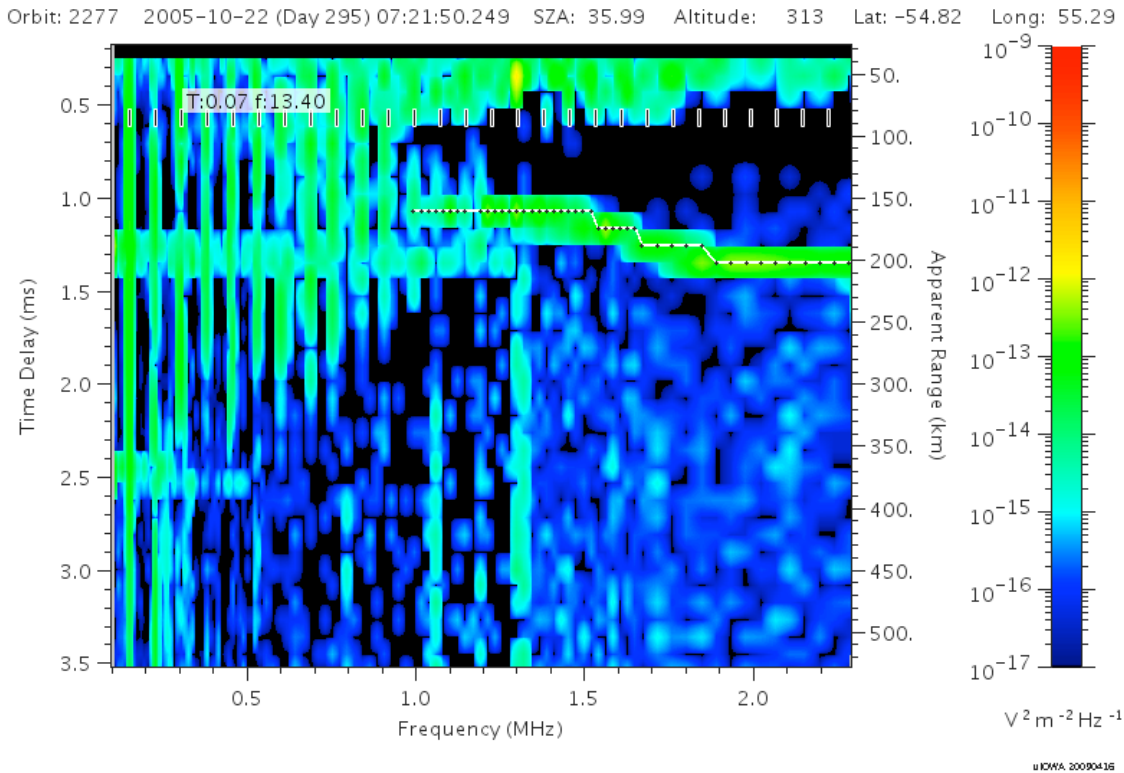


Fig. 4. An expanded portion of Fig. 1. The frequencies of the plasma oscillation frequencies are indicated by the short dark lines coinciding with the bright vertical bands. The best way to measure the local plasma frequency is to find the average difference in frequency between these harmonics. The plasma

frequency in Fig. 1 is measured to be 0.075 MHz. The ionospheric trace, measured using an intensity threshold, is shown as a white and black dotted line.

One of the early discoveries from MARSIS was that the instrument often recorded harmonics of the plasma oscillations occurring close to the Mars Express spacecraft. The instrument is sensitive to the oscillations occurring in the plasma. Because the oscillations are quite intense, they can cause nonlinear distortion in the instrument receiver, causing the receiver to record the existence of these harmonics, even though they do not actually exist in the plasma. These harmonics, which are visible in Fig. 4 as vertical high-intensity stripes, are easily exploited by measuring their average frequency separation to make a reasonably accurate measurement of the plasma frequency in the vicinity of the spacecraft. In Fig. 4, the plasma frequency is measured to be 0.075 MHz.

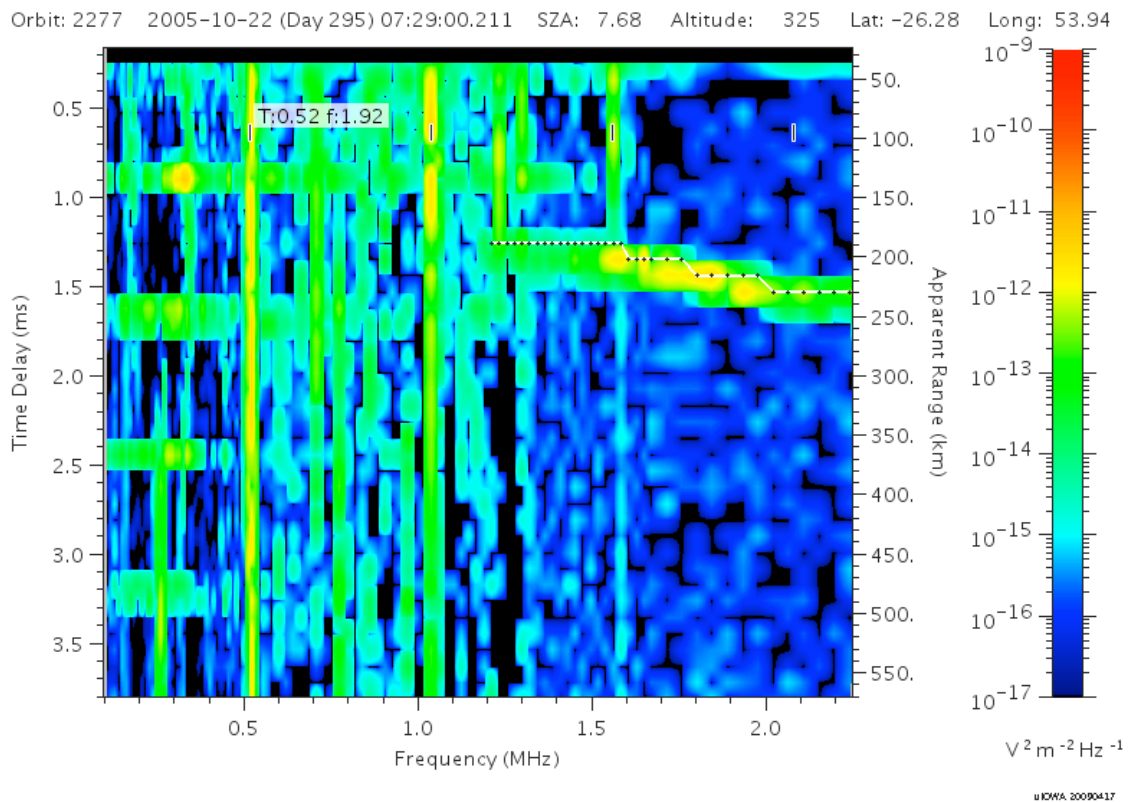


Fig. 5. The plasma frequency is measured from the frequency difference between the bright vertical bands to be 0.521 MHz. Using the faint lines with the bright lines gives a result about $\frac{1}{2}$ of that.

A reasonable estimate of the error can be made by referring to Fig. 2. The spacing between sampling frequencies at frequencies below 0.7 MHz (about the upper limit of the measured plasma frequency) varies between about 2 and 10%. The upper limit on the uncertainty comes down to about 3% if the number of visible harmonic lines is treated as the number of independent samples.

Figure 5 illustrates one of the ambiguities of this method. In this figure, there is a set of bright plasma harmonics and slightly fainter harmonics between the bright ones. If the bright lines are used to indicate the plasma oscillation harmonics, the plasma frequency is measured as 0.521 MHz; if the fainter lines are included, the plasma frequency will be half of that or less. One reason that there might be intermittent faint lines between the brighter lines is that the spacecraft occasionally passes through regions in which the density goes through a rapid transition. Such an occurrence is quite possible because the spacecraft is traveling at approximately 4 km/s at altitudes where data are being taken, which translates to a distance of about 30 km in the 7.543 s between ionograms, or about 5 m in the 1.26 s it takes to collect data for a single ionogram. One way to check which set of harmonics is most valid is to examine the ionograms immediately before and after the ionogram in question; however, it is not always clear which set of lines is correct. Where there is a clear distinction between brighter and fainter harmonic lines, the usual practice has been to use the brighter set of lines.

There are times when the plasma oscillation harmonics are not available, as for example, when the spacecraft is in the shocked solar wind (see Duru et al. 2008). In such cases, the best independent guess of the plasma frequency at the spacecraft is usually the best that can be done. A value interpolated from surrounding measurements is a possibility that should be used with caution because of the inherent variability of the measurement. If the spacecraft is in the solar wind, the local plasma frequency can be independently estimated with some justification.

IV. The Ionospheric Trace

In this section we shall describe the process for taking the ionospheric trace, i. e., getting the delay time of the sounding wave reflected from the ionosphere as a function

of the sounding frequency. To start, we should note that this activity is the greatest contributor to uncertainty in the final result. Uncertainty in the spacecraft-local plasma frequency is typically 3% or less, while uncertainty in the elements of the trace is one pixel = $\sigma R_{\text{app}} = c \sigma t_{\text{delay}}/2 = c \times 91.4 \mu\text{s}/2 \approx 13.7 \text{ km}$, which is approximately 10% of the ionospheric peak altitude. Because of the sharp fall-off in transmitted power inherent in a dipole antenna, frequencies below 1 MHz can be undetectably faint and are frequently swamped by noise. Because of this problem, it is not yet possible to completely automate the system for taking an ionospheric trace. In this manual, we will describe the simplest method for a person sitting at a computer screen using display software that includes a readable cursor.

Consider that the transmitted sounding wave has a small but measureable rise-time. An example of the rise in amplitude of the sounding wave is given in Fig. 6. This figure shows the history of the transmitted voltage pulse on the antenna for a sampling of frequencies as measured in the engineering laboratory and captured on an oscilloscope screen. At all frequencies, the wave is at over half its final amplitude after approximately 3 μs , which translates to an error of about 0.45 km in apparent range. Since one pixel represents an uncertainty of approximately $\pm 6.9 \text{ km}$, this effect is negligible.

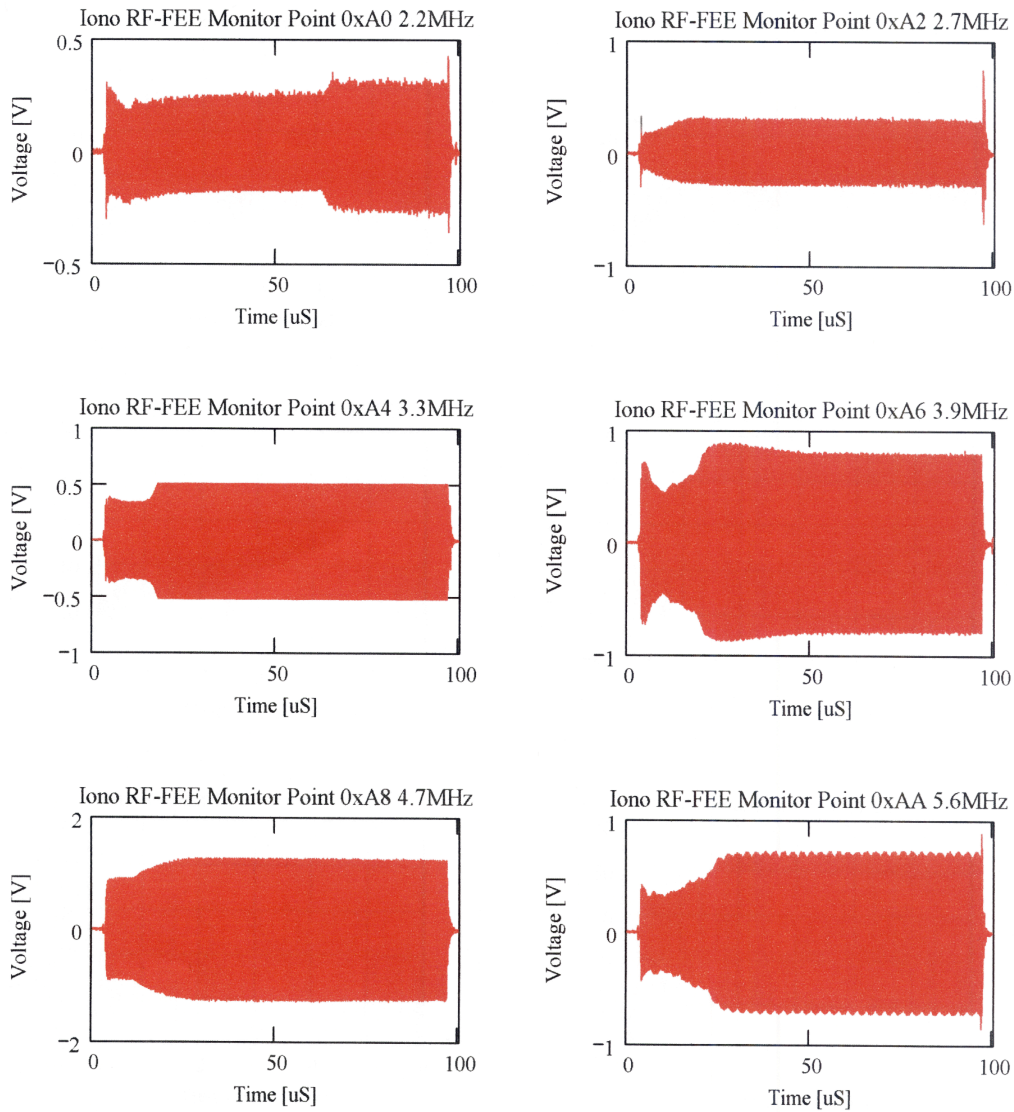


Fig. 6. Evolution of the sounding wave amplitude on the MARSIS antenna measured in the engineering laboratory and captured on an oscilloscope. At all frequencies the wave is at greater than $\frac{1}{2}$ amplitude by 3 μ s after the impulse commences.

Before starting to make a trace, one should note, *e. g.*, from Fig. 1, that the ionospheric reflection as seen on an ionogram has a finite width. Because the zero of the time measurement is the beginning of the transmitted sounding pulse, ideally one would take the measurement of the reflected trace at the leading edge of the reflection.

However, because the worker is using an averaged ionogram displayed on a computer screen, the visual upper limit of the trace is likely to be too short an estimate.

Two conventions have been used to determine the time delay. One method is to choose a threshold value of the intensity to define the upper edge of the ionospheric reflection. This value must be chosen empirically and is therefore somewhat arbitrary. This method also suffers from a slight bias along the trace because the reflected intensity decreases at low frequencies. A better defined marker is the uppermost maximum intensity value of the ionospheric reflection. In practice, because of the rather coarse resolution in time delay, the threshold and maximum methods agree roughly half the time. When they disagree, the maximum method gives a value that is longer by one pixel = 91.4 μs .

The choice of criterion for determination of the trace position will depend on the software available to the worker. If digital values of the intensity are available, it is easy to use a threshold criterion. If the traces are made on the basis of a visual determination of brightness, then the trace maximum provides a more consistent standard. If one uses the maximum brightness as the tracing criterion, it can be reconciled on average with the results of the threshold method by subtracting $\frac{1}{2}$ pixel, or 45.7 μs , from each delay time.

This procedure is equivalent to treating the center time of the transmitted pulse as the zero time. Because this correction is less than the error on the measurement, it is not usually considered necessary.

In Fig. 1 the ionospheric trace is made using a threshold of $1 \times 10^{-15} \text{ (V/m)}^2/\text{Hz}$. It can be seen that in most cases this threshold is in the visual center of the reflection and close to the position of maximum brightness of the trace.

A procedure for taking the trace is as follows:

1. Display desired ionogram on a computer monitor.
2. Determine the lowest frequency where the ionospheric trace is distinguishable from noise.
3. Use the cursor to digitize delay times for all sampled frequencies by either the threshold or maximum intensity method depending on available facilities.

The resulting data should consist of a list of sounding frequencies and a corresponding list of delay times. These data will serve as input to the smoothing and inversion phases of the electron density profile process.

V. Processing of the Ionospheric Trace.

It should be noticed that MARSIS ionograms are typically noisy at frequencies below 1 MHz. In particular, there are several strong interference frequencies that will corrupt the digitized trace in the case where an automated procedure is used to do the measurement. A trace done by an automated method must always be examined for corruption due to noise or interference. If the trace is done visually, this step will be incorporated into the data taking procedure.

The somewhat coarse resolution of the time delay measurements implies that the plot of delay time versus sounding frequency will have a quantized, or “stair step,” appearance to it. Although this irregularity is not a serious impediment to a useful inversion of the ionospheric trace, it is marginally more precise to smooth out these results. There are various algorithms for performing this operation; however, since it is not considered essential, we do not include such an algorithm here. Again, this step is only necessary if the data are taken by an automated procedure; a person using a visual method can effectively smooth the result by eye.

VI. Inversion Routine

The purpose of the previous four sections is to acquire a reliable value of the time delay as a function of the sounding frequency. The resulting function can then be inverted to get the profile of electron density as a function of altitude. The process makes a number of assumptions:

1. Propagation along the nadir direction.
2. Plane parallel stratification of the ionosphere.
3. Nonmagnetic plasma dispersion relation.
4. Monotonic profile.

Condition 1 is known to be violated in the case of structures in the ionosphere associated with cusp regions between crustal magnetic structures (Duru et al., 2006, Nielsen et al., 2007). Furthermore, unpublished work indicates that off-nadir propagation may affect the ionospheric trace more commonly than is currently supposed; however, of these assumptions, the most commonly violated in an obvious way is the last. Cusps are often visible in the ionospheric trace at low sounding frequencies and altitudes much higher than the peak [see, *e. g.*, Kopf *et al.* (2008)]. Figure 7 shows an example of a “cusp-like” ionospheric trace. Other examples can be found in work by Kopf *et al.* (2008) and Wang *et al.* (2009). In these cases, specialized methods are needed to invert the trace [see, *e. g.*, Wang *et al.* (2009)]. In this manual, we will only deal with the simplest case, in which the physical profile can reasonably be assumed to be monotonic.

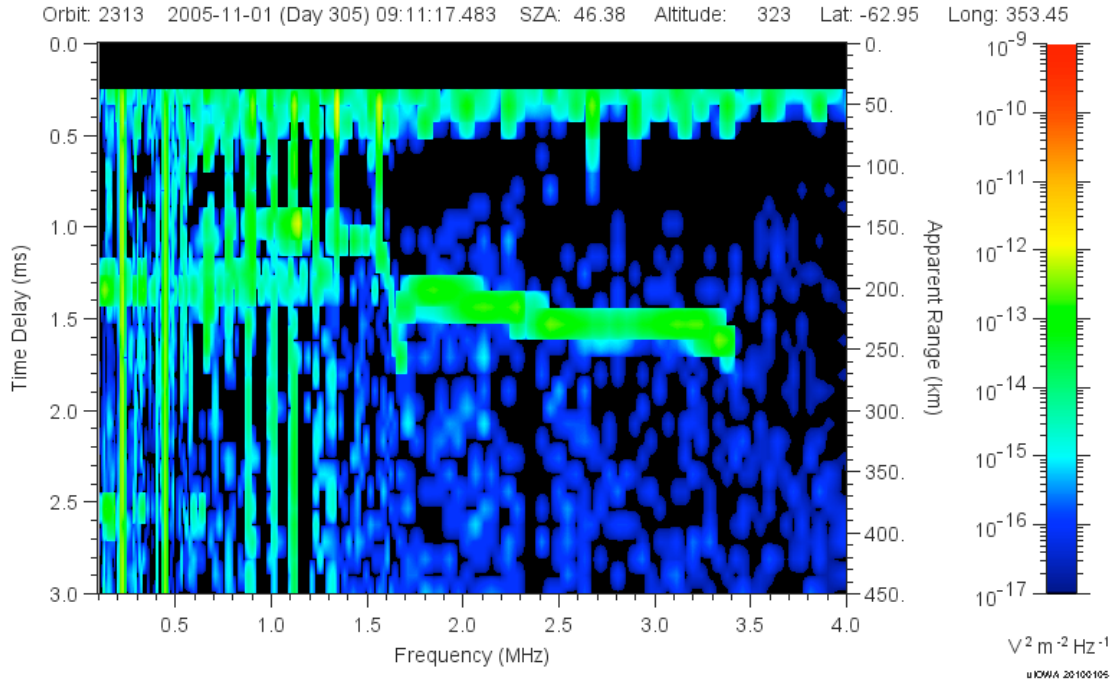


Fig. 7. Ionogram showing “cusp-like” non-monotonic ionospheric trace. The cusp can be seen near frequency 1.6 MHz and between time delays of 1.3 and 1.8 ms.

The integral equation to be inverted is given by

$$\tau_i = 2 \int_0^z \frac{dz}{V_g} = 2 \int_0^z \frac{dz}{c \sqrt{1 - \left(\frac{f_{pe}(z)}{f_{s,i}} \right)^2}} \quad (1)$$

where the group velocity, from the dispersion relation for propagation of an electromagnetic wave in a nonmagnetic plasma is given by the denominator of Eq. (1). In Eq. (1), z stands for the range from the spacecraft in the nadir direction. The factor of 2 is because the sounding wave travels in both directions. The subscript i indexes the sounding frequency, so that τ_i stands for the delay time measured for the sounding frequency $f_{s,i}$. Equation (1) must be solved for z , the range from the spacecraft to the reflection point.

The solution to equation (1) can be carried out in a number of ways. The classical solution is called Abel's transformation and yields the solution

$$z(f_n) = \frac{2}{\pi} \int_{\alpha_0}^{\pi/2} \frac{c}{2} \tau(f_n \sin \alpha) d\alpha \quad (2)$$

where f_n is the frequency for which we wish to compute the range from the spacecraft and $\sin(\alpha_0)$ is equal to f_0/f_n . A derivation of Eq. 2 is given by Budden (1961). In this formulation, f_n and τ are thought of as continuous functions. The profile of τ as a function of f_n can easily be converted to a continuous function; however, it is convenient to skip this step by solving equation (1) by explicitly assuming a functional form for $f_{pe}(z)$ and stepwise solving equation (1) over discrete intervals in z . Because this method involves solution layer-by-layer, it is called the ‘‘lamination’’ method. Thorough outlines of the application of the classic lamination method—widely used in the analysis of ground-based ionograms—to MARSIS topside sounding ionograms, can be found in papers by Zou and Nielsen (2004), Nielsen *et al.* (2006), and Morgan *et al.* (2008).

The lamination method involves dividing the ionosphere into plane parallel strata at points where data are taken. If we compute the integral for the i th data point, then we are integrating from the zeroth point (*i. e.*, the position of the spacecraft) to data point i . The ray path integral can be rewritten as a sum

$$\tau_i = \frac{2}{c} \sum_{j=1}^{j=i} \int_{z_{j-1}}^{z_j} \frac{dz}{\sqrt{1 - (f_{pe}(z)/f_{s,i})^2}} = \sum_{j=1}^{j=i} \Delta\tau_{i,j} \quad (3)$$

The two commonly used functional forms assumed for the values of $f_{pe}(z)$ in the denominator of Eq. (3) are linear and exponential. Because the form of the electron density profile in the large gap between the spacecraft position and the first reflection point is thought on average to be of exponential form (see Duru *et al.*, 2008), we here

give that version. This allows the investigator to use a single process to compute the whole profile rather than finding an exponential for the first segment and the linear formulation for the rest. Aside from this matter of convenience, neither method has an advantage over the other.

Over the j th interval, from data point $j-1$ to data point j , we assume that the plasma frequency has the form

$$f_{pe}(z) = f_{pe, j-1} \exp(\alpha_j z) \quad (4)$$

which can be inverted to

$$z = \frac{1}{\alpha_j} \ln \frac{f_{pe}}{f_{pe, j-1}} \quad (5)$$

This relation enables us to change variables from z to f_{pe}

$$\Delta \tau_{i, j} = \int_{f_{pe, j-1}}^{f_{pe, j}} \frac{1}{\alpha_j f_{pe}} \frac{df_{pe}}{c \sqrt{1 - (f_{pe}/f_{s, i})^2}} \quad (6)$$

If we make the further change of variable $f_{pe}/f_{s, i} = \sin \theta$, then the j th term of the i th delay time becomes

$$\Delta \tau_{i, j} = \frac{2}{c} \int_{\theta_{i, j-1}}^{\theta_{i, j}} \frac{1}{\alpha_j f_{s, i} \sin \theta} \frac{f_{s, i} \cos \theta d\theta}{\cos \theta} = \frac{2}{\alpha_j c} \int_{\theta_{i, j-1}}^{\theta_{i, j}} \frac{d\theta}{\sin \theta} \quad (7)$$

where $\theta_{i, j} = \arcsin(f_{pe, j}/f_{s, i})$. The integral in Eq. (6) can be computed by elementary methods to get

$$\Delta \tau_{i, j} = \frac{1}{2} \frac{2}{c \alpha_j} \ln \left[\frac{\left(\left(1 - \sqrt{1 - (f_{pe, j}/f_{s, i})^2} \right) \left(1 + \sqrt{1 - (f_{pe, j-1}/f_{s, i})^2} \right) \right)}{\left(\left(1 - \sqrt{1 - (f_{pe, j-1}/f_{s, i})^2} \right) \left(1 + \sqrt{1 - (f_{pe, j}/f_{s, i})^2} \right) \right)} \right]$$

Noting that the $f_{pe, j}$'s are just the sounding frequencies intermediate between the spacecraft, index 0, and the desired data point i , everything in this expression is either a measured time delay or a fixed frequency except the exponential coefficients α_j . If we insert these values into equation (3), we find

$$\tau_i = \sum_{j=1}^{j=i} \frac{1}{c\alpha_j} \ln \frac{\left[\left(1 - \sqrt{1 - (f_{pe,j} / f_{s,i})^2}\right) \left(1 + \sqrt{1 - (f_{pe,j-1} / f_{s,i})^2}\right) \right]}{\left[\left(1 - \sqrt{1 - (f_{pe,j-1} / f_{s,i})^2}\right) \left(1 + \sqrt{1 - (f_{pe,j} / f_{s,i})^2}\right) \right]} \quad (8)$$

If there are n sounding frequencies, then this set of equation constitutes a linear system of n equations in n variables α_j . The system can be efficiently solved by starting with $i=1$, solving for α_1 , and using this value in the $i=2$ equation, proceeding through $i=n$. A piece of IDL code which has been found useful is included below.

```

pro range_exp_comp, freq_arr_mhz, time_arr_msec, range_exp

c_kmps=3.e5
n_freqs=n_elements(freq_arr_mhz)

range_exp=dblarr(n_freqs)
alpha_arr=dblarr(n_freqs)
freq_rat=dblarr(n_freqs,n_freqs)
diff_exp=dblarr(n_freqs,n_freqs)

freq_arr=freq_arr_mhz*1e6
l_rat_freq=log(freq_arr(1:*)/freq_arr)
time_arr=(time_arr_msec)*1e-3/2.0
time_arr(0)=0.
app_range=c_kmps*time_arr
for i=1,n_freqs-1 do begin
    freq_rat(i,0:i)=freq_arr(0:i)/freq_arr(i)
endfor
freq_rat=asin(freq_rat)
for i=1,n_freqs-1 do begin
    freq_rat(i,i)=!dpi/2.d0
endfor
cos_f=cos(freq_rat)
exp_weight=0.5*log((1.d0-cos_f)/(1.d0+cos_f))
for i=1,n_freqs-1 do begin
    diff_exp(i,1:i)=exp_weight(i,1:i)-exp_weight(i,0:i-1)
endfor
alpha_arr(1)=-diff_exp(1,1)/app_range(1)
for i=2,n_freqs-1 do begin
    alpha_arr(i)=-diff_exp(i,i)/ $
        (app_range(i)+total((diff_exp(i,1:i-1)/alpha_arr(1:i-1))))
endfor
range_exp(0)=0.0d0
for i=1,n_freqs-1 do begin
    range_exp(i)=range_exp(i-1)-l_rat_freq(i-1)/alpha_arr(i)
endfor

end

```

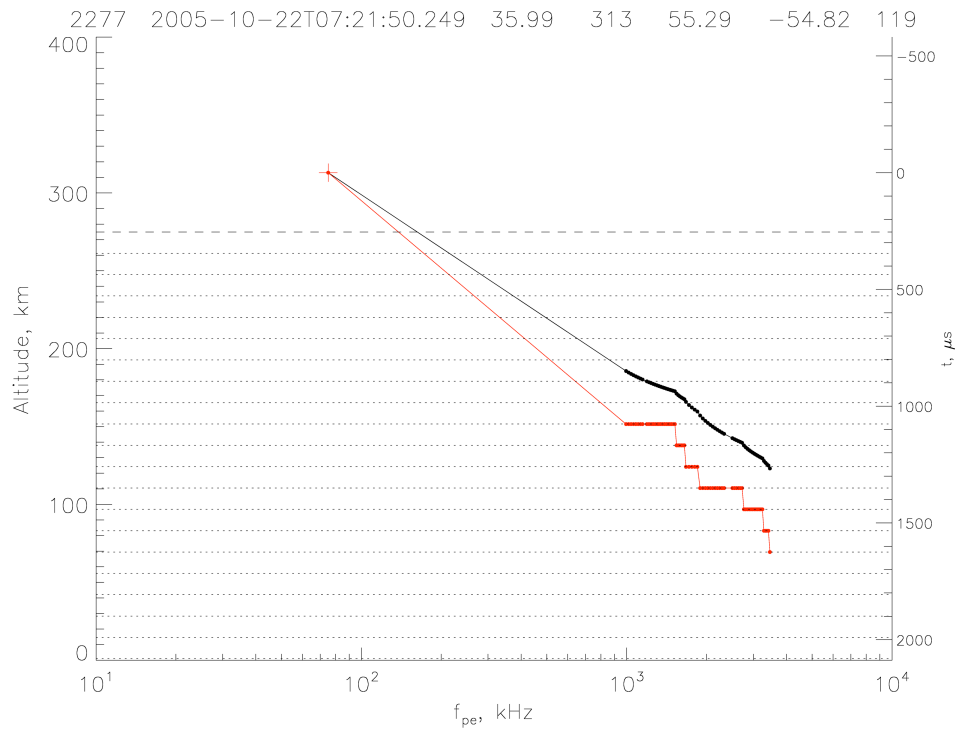


Fig. 8. Red: Ionospheric trace shown in Fig. 1. Black: Ionospheric trace corrected for dispersion according to Equation (8). The x-axis shows the ionospheric plasma frequency, which is sampled at the instrumental sounding frequencies. The left-hand y-axis shows the altitude, apparent (black) and corrected (red). The right-hand y-axis, which applies only to the apparent (red) trace, gives the measured delay time. The horizontal grid lines indicate the sampled delay times.

Inputs are `freq_arr_mhz`, the sampled frequencies in MHz, and `time_arr_msec`, measured delay times in ms. The output is `range_exp`, computed range from the spacecraft in km. The spacecraft altitude is needed to compute the altitude. The zeroeth element of `freq_arr_mhz` should be the spacecraft altitude. The zeroeth element of `time_arr_msec` should be 0.

The effect of using Eq. (8) on the trace shown in Fig. 1 is shown in Fig. 8. The red trace in this figure shows the data points as taken from the array shown in Fig. 1. The black trace is the electron density profile, corrected for dispersion using Eq. 8. Results of this computation are shown in Table 2.

Table 2

Orbit 2277: 072150, Nielsen 119

Snding frq MHz	Del time ms	App range km	SC Alt km	n_e cm ⁻³	Crt range km	Crt alt km
0.075	0.000e+00	0.000	313.000	6.98e+01	0.000	313.000
0.995	1.077e+00	161.437	313.000	1.23e+04	127.360	185.640
1.017	1.077e+00	161.437	313.000	1.28e+04	128.325	184.675
1.039	1.077e+00	161.437	313.000	1.34e+04	129.206	183.794
1.061	1.077e+00	161.437	313.000	1.40e+04	130.023	182.977
1.083	1.077e+00	161.437	313.000	1.45e+04	130.788	182.212
1.105	1.077e+00	161.437	313.000	1.51e+04	131.508	181.492
1.127	1.077e+00	161.437	313.000	1.58e+04	132.188	180.812
1.148	1.077e+00	161.437	313.000	1.63e+04	132.804	180.196
1.192	1.077e+00	161.437	313.000	1.76e+04	133.996	179.004
1.214	1.077e+00	161.437	313.000	1.83e+04	134.556	178.444
1.236	1.077e+00	161.437	313.000	1.89e+04	135.091	177.909
1.258	1.077e+00	161.437	313.000	1.96e+04	135.602	177.398
1.280	1.077e+00	161.437	313.000	2.03e+04	136.092	176.908
1.302	1.077e+00	161.437	313.000	2.10e+04	136.562	176.438
1.323	1.077e+00	161.437	313.000	2.17e+04	136.994	176.006
1.345	1.077e+00	161.437	313.000	2.24e+04	137.429	175.571
1.367	1.077e+00	161.437	313.000	2.32e+04	137.848	175.152
1.389	1.077e+00	161.437	313.000	2.39e+04	138.252	174.748
1.411	1.077e+00	161.437	313.000	2.47e+04	138.641	174.359
1.433	1.077e+00	161.437	313.000	2.55e+04	139.017	173.983
1.455	1.077e+00	161.437	313.000	2.63e+04	139.380	173.620
1.476	1.077e+00	161.437	313.000	2.70e+04	139.715	173.285
1.498	1.077e+00	161.437	313.000	2.78e+04	140.055	172.945
1.520	1.077e+00	161.437	313.000	2.87e+04	140.384	172.616
1.542	1.168e+00	175.077	313.000	2.95e+04	141.856	171.144
1.564	1.168e+00	175.077	313.000	3.03e+04	142.829	170.171
1.586	1.168e+00	175.077	313.000	3.12e+04	143.619	169.381
1.608	1.168e+00	175.077	313.000	3.21e+04	144.308	168.692
1.630	1.168e+00	175.077	313.000	3.29e+04	144.931	168.069
1.651	1.168e+00	175.077	313.000	3.38e+04	145.480	167.520
1.673	1.260e+00	188.868	313.000	3.47e+04	147.137	165.863
1.717	1.260e+00	188.868	313.000	3.66e+04	149.170	163.830
1.761	1.260e+00	188.868	313.000	3.85e+04	150.780	162.220
1.805	1.260e+00	188.868	313.000	4.04e+04	152.159	160.841
1.848	1.260e+00	188.868	313.000	4.23e+04	153.357	159.643
1.892	1.351e+00	202.508	313.000	4.44e+04	155.941	157.059
1.936	1.351e+00	202.508	313.000	4.65e+04	157.798	155.202
1.980	1.351e+00	202.508	313.000	4.86e+04	159.351	153.649
2.023	1.351e+00	202.508	313.000	5.08e+04	160.691	152.309
2.067	1.351e+00	202.508	313.000	5.30e+04	161.930	151.070
2.111	1.351e+00	202.508	313.000	5.53e+04	163.065	149.935
2.155	1.351e+00	202.508	313.000	5.76e+04	164.116	148.884
2.198	1.351e+00	202.508	313.000	5.99e+04	165.074	147.926
2.242	1.351e+00	202.508	313.000	6.23e+04	165.993	147.007
2.286	1.351e+00	202.508	313.000	6.48e+04	166.858	146.142
2.330	1.351e+00	202.508	313.000	6.73e+04	167.675	145.325
2.505	1.351e+00	202.508	313.000	7.78e+04	170.481	142.519
2.548	1.351e+00	202.508	313.000	8.05e+04	171.113	141.887
2.592	1.351e+00	202.508	313.000	8.33e+04	171.728	141.272

2.636	1.351e+00	202.508	313.000	8.62e+04	172.315	140.685
2.680	1.351e+00	202.508	313.000	8.91e+04	172.878	140.122
2.723	1.351e+00	202.508	313.000	9.19e+04	173.405	139.595
2.767	1.442e+00	216.149	313.000	9.49e+04	175.142	137.858
2.811	1.442e+00	216.149	313.000	9.80e+04	176.341	136.659
2.855	1.442e+00	216.149	313.000	1.01e+05	177.337	135.663
2.898	1.442e+00	216.149	313.000	1.04e+05	178.200	134.800
2.942	1.442e+00	216.149	313.000	1.07e+05	179.005	133.995
2.986	1.442e+00	216.149	313.000	1.11e+05	179.752	133.248
3.030	1.442e+00	216.149	313.000	1.14e+05	180.452	132.548
3.073	1.442e+00	216.149	313.000	1.17e+05	181.097	131.903
3.117	1.442e+00	216.149	313.000	1.20e+05	181.724	131.276
3.161	1.442e+00	216.149	313.000	1.24e+05	182.321	130.679
3.205	1.442e+00	216.149	313.000	1.27e+05	182.891	130.109
3.248	1.442e+00	216.149	313.000	1.31e+05	183.425	129.575
3.292	1.534e+00	229.939	313.000	1.34e+05	185.078	127.922
3.336	1.534e+00	229.939	313.000	1.38e+05	186.233	126.767
3.380	1.534e+00	229.939	313.000	1.42e+05	187.200	125.800
3.423	1.534e+00	229.939	313.000	1.45e+05	188.041	124.959
3.467	1.625e+00	243.579	313.000	1.49e+05	189.918	123.082

VII. Some Caveats

It will be noticed in Figs. 1, 4, and 5 that there is usually a large space in both frequency and delay time between the spacecraft-local measurement and the first sounding point. The reason for this recurring data gap is that the strength of the sounding wave decreases sharply at low frequency, a characteristic of transmission from a dipole antenna. This low-frequency gap in the measurements is the weakest link in the process of acquiring electron density profiles from MARSIS sounding traces. As explained in the previous section, the solution of all practitioners so far has been to assume an exponential fall-off with increasing altitude. This appears to be a good assumption *on average*. The work of Duru *et al.* (2008), using statistical analysis of the local plasma frequency measurements over a wide range of altitudes and solar zenith angles bears out the assumption of exponential decrease with altitude; however, this work is limited to the range in which the local plasma frequency is available. These authors showed that, when the spacecraft is outside the ionosphere and in the shocked solar wind, the harmonics on which the local plasma frequency is based are usually not available. Furthermore, at large spacecraft altitudes the assumption of a single exponential is increasingly problematic. Inversions of traces taken at high altitude should be treated with caution.

Another area for caution is that a sounder cannot get a reflection from under a shelf or overhang in the plasma density. It is for this reason that the X-ray induced “M1” layer at about 90-100 km altitude is never detected by MARSIS. In addition, cusps similar to that visible at the peak plasma frequency are often visible at higher altitudes, indicating that there is a shelf in the ionospheric structure [see, *e. g.*, Kopf *et al.* (2008)]. The inversion process as outlined in Section VI cannot take these structures into account and some assumptions must be made. Procedures for doing this are outlined by Budden (1961). Wang *et al.* (2009) have performed inversions on such profiles.

One good aspect of the sounding data is that, to some extent, the inversion process is self correcting. Equation (1) shows that the correction for dispersion becomes vanishingly small as the sounding frequency becomes much larger than the plasma frequency of the medium through which it is traveling. Thus, the dispersion correction is largely due to plasma in the vicinity of the reflection point.

References

Budden, K. G. (1961), *Radio Waves in the Ionosphere*, Cambridge Univ. Press, Cambridge, U. K.

Duru, F., D. A. Gurnett, T. F. Averkamp, D. L. Kirchner, R. L. Huff, A. M. Persoon, J. J. Plaut, and G. Picardi (2006), Magnetically controlled structures in the ionosphere of Mars, *J. Geophys. Res.*, 111, A12204, doi: 10.1029/JA011975.

Duru, F., D. A. Gurnett, D. D. Morgan, R. Modolo, A. F. Nagy, and D. Najib, Electron densities in the upper ionosphere of Mars from the excitation of electron plasma oscillations (2008), *J. Geophys. Res.*, 113, A07302, doi:10.1029/2008JA013073.

Kopf, A. J., D. A. Gurnett, D. D. Morgan, D. L. Kirchner (2008), Transient layers in the topside ionosphere of Mars, *Geophys. Res. Lett.*, 35, L17102, doi:10.1029/2008GL034948.

Morgan, D. D., D. A. Gurnett, D. L. Kirchner, J. L. Fox, E. Nielsen, and J. J. Plaut, Variation of the Martian ionospheric electron density from Mars Express radar soundings (2008), *J. Geophys. Res.*, *113*, A09303, doi:10.1029/2008JA013313.

Nielsen, E., H. Zou, D. A. Gurnett, D. L. Kirchner, D. D. Morgan, R. Huff, R. Orosei, A. Safaeinili, J. J. Plaut, and G. Picardi (2006), Observations of vertical reflections from the topside Martian ionosphere, *Space Sci. Rev.* *126*, 373-388, doi:10.1007/s11214-006-9113-y.

Nielsen, E., X.-D. Wang, D. A. Gurnett, D. L. Kirchner, R. Huff, R. Orosei, A. Safaeinili, J. J. Plaut, and G. Picardi (2007), Vertical sheets of dense plasma in the topside Martian ionosphere, *J. Geophys. Res.*, *112*, E02003, doi: 10.1029/2006JE002723.

Wang, X.-D., J.S. Wang, E. Nielsen, and H. Zou, "Hook" structure in MARSIS ionogram and its interpretation (2009), *Geophys. Res. Lett.*, *36*, L13103, doi:10.1029/2009GL038844.

Zou, H. and E. Nielsen, Methods for obtaining electron density profiles from MARSIS ionograms and derivation of parameters characterizing the profiles (2004). MPAe-W-485-04-01 (Max-Planck-Institut internal document).